Frontiers in Heat and Mass Transfer

Available at www.ThermalFluidsCentral.org

NUMERICAL STUDY ON HEAT TRANSFER CHARACTERISTICS OF PROPYLENE GLYCOL-WATER MIXTURE IN SHELL SIDE OF SPIRAL WOUND HEAT EXCHANGER

Xiaoyong Gu[*], Guohe Jiang, Yang Wo, Biwen Chen

Merchant Marine College, Shanghai Maritime University, Shanghai, 201306, China

ABSTRACT

The heat transfer characteristics of propylene glycol-water (PG-W) mixture with different concentrations in shell side of spiral wound heat exchanger (SWHE) with different geometric parameters were studied numerically. Experiment was carried out and the average difference between the simulated results and the experimental results was 5.3%. The simulation results show that heat transfer coefficient increases with the increase of center core diameter and longitudinal spacing of tubes, but decreases with the increase of tube outer diameter. The center core diameter and tube outer diameter have greater effects on heat transfer performances at higher concentration. Economic index was established and found that adding materials for changing center core diameter and tube outer diameter will improve economic index. While adding materials for changing longitudinal spacing of tubes will reduce economic index. Adding materials for changing center core diameter has higher cost performance. The results can provide reference for the design of gasifier in the gas supply system of dual fuel engine.

Keywords: *Propylene glycol-water mixture, heat transfer coefficient, spiral wound heat exchanger, numerical simulation.*

1. INTRODUCTION

Dual-fuel engines using natural gas have a broad application prospect on ships because very little sulphur dioxide was emitted (Mestemaker *et al*., 2020). To facilitate storage, natural gas is stored generally in tanks in liquid form, when it is needed, a hot fluid will gasify it (Park *et al*., 2018). In order to reduce the risk of hot fluid solidification in the gasifier, fluid with low melting point is appropriate. Considering the cost at the same time, propylene glycol-water (PG-W) mixture is an ideal fluid (Klotzbücher *et al*., 2007). Due to the small space on the ship, the gasifier should be small and efficient, the spiral wound heat exchanger (SWHE) is an ideal gasifier (Weikl *et al*., 2014; Mirgolbabaei, 2018). In a SWHE, multiple tubes are wound on a cylinder, and the winding direction of adjacent tubes is opposite. One fluid flows through the tubes and the other fluid flows through the shell side (Wang *et al*., 2018). Compared with other heat exchangers, the SWHE has a larger heat transfer area with a smaller volume. The shape of the tubes can be round, elliptical or other shapes (Wang *et al*., 2019).

There are amounts of researches on SWHE. By using helium as working medium, Abolmaali et al. (2019) studied the effects of the number of tubes in the first layer, the number of layers and tube outer diameter on heat transfer coefficient. The conclusions show that the number of tubes in the first layer was the only parameter that has no influence on heat transfer coefficient. By using ethane, propane, methane/ethane mixture, ethane/propane mixture and ethane/butane mixture as working media, Neeraas et al. (2004) measured their heat transfer coefficients in SWHE. Using water as working medium, Ahmadi (2018) studied the influence of winding diameter and diameter of tubes on heat transfer coefficient, concluded that winding diameter had a great influence on heat transfer coefficient. Daghigh et al. (2018) studied the heat transfer coefficient of propylene glycol-water mixture with a concentration of 70% in winding tube, and concluded that the heat transfer efficiency of propylene glycol-water mixture in conical-

cylindrical spiral coil was higher than that in cylindrical spiral coil. Gupta et al. (2014) conducted an experimental study on the heat transfer characteristics of R134a in different heat exchangers and evaluated the advantages of SWHE over straight tube heat exchanger. Solanki et al. (2019) studied the condensation of R600a in smooth spiral tube and corrugated spiral tube. It was concluded that the R600a in corrugated spiral tube had higher heat transfer efficiency. Pawar et al. (2014) studied the heat transfer characteristics of water and glycerol - water mixture in SWHE through experiment. Saydam et al. (2019) designed a SWHE and carried out experiments with ethylene glycol solution as working medium. It was concluded that energy recovery efficiency increases with the increase of flow. Ghorbani et al. (2010) studied the effects of different diameters of tube and Re on the heat transfer coefficient of water in SWHE, and summarized that the equivalent diameter of the shell was the best characteristic length. Yu et al. (2018) numerically studied the condensation of mixed hydrocarbon refrigerants in helical tubes. It was concluded that the diameter of tube and mass flow had the greatest influence on the heat transfer coefficient. Mirgolbabaei (2018) evaluated the thermal performance of SWHE at different coil-to-tube diameter ratios and different dimensionless coil pitch. In addition, the heat transfer characteristics of the fluid in shell side under vibration and rolling were studied (Zhu *et al*., 2019; Duan *et al*., 2016).

The structure of SWHE is relatively complex, and the heat transfer coefficient of working medium flowing in the shell side depends not only on SWHE's structure, but also on the material properties of working medium. In this paper, PG-W mixture with three concentrations were used as working medium in the shell side of SWHE, and the effects of center core diameter, longitudinal spacing of tubes and tube outer diameter on heat transfer coefficient were investigated by numerical simulation. The economic index was established to evaluate the economy of SWHE. It provides reference for the optimal design of gasifier for dual fuel engine.

---

* *Corresponding author. Email: guxy9011@163.com*

2. NUMERICAL SIMULATION

2.1 Physical model

The SWHE is shown in Fig. 1(a) and Fig. 1(b). Since the SWHE is complex, it is simplified. The simplified SWHE is shown in Fig. 1 (c) and Fig. 1(d).

(a) SWHE (b) Flow direction of working fluid

(c) Simplified SWHE (d) Profile of SWHE
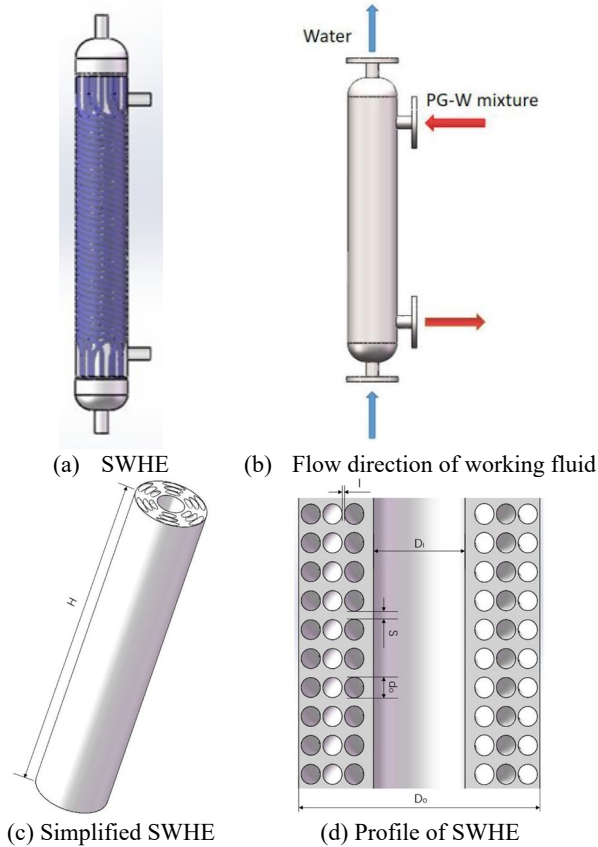
Fig. 1 Physical model of SWHE

The length of SWHE, the outer diameter of SWHE and the horizontal spacing of tubes were kept unchanged, the center core diameter, the longitudinal spacing of tubes and the tube outer diameter were changed. The specific parameters are shown in table 1.

Table 1 Parameters of SWHE

Parameters	Value
Length of SWHE (H, mm)	450
Outer diameter of SWHE (D_o, mm)	100
Horizontal spacing of tubes (l, mm)	1
Center core diameter (D_i, mm)	32, 35, 38, 41, 44
Longitudinal spacing of tubes (S, mm)	2, 3, 4, 5, 6
Tube outer diameter (d_o, mm)	6, 7, 8, 9, 10

2.2 Numerical methods

The Realizable k-ε turbulence model was adopted for calculation process. The basic equations include mass, momentum and energy equations.

Momentum equation:

$$\frac{\partial}{\partial x_i}(\rho u_i u_k) = \frac{\partial}{\partial x_i}\left(\mu \frac{\partial u_k}{\partial x_i}\right) - \frac{\partial P}{\partial x_k} \tag{1}$$

Energy equation:

$$\frac{\partial}{\partial x_i}(\rho u_i t) = \frac{\partial}{\partial x_i}\left(\frac{\lambda}{c_p}\frac{\partial t}{\partial x_i}\right) \tag{2}$$

Continuity equation:

$$\frac{\partial}{\partial x_i}(\rho u_i) = 0 \tag{3}$$

Equation of turbulent kinetic energy:

$$\frac{\partial}{\partial t}(\rho k) + \frac{\partial}{\partial x_j}(\rho k u_i) = \frac{\partial}{\partial x_j}\left[\left(\mu + \frac{\mu_t}{\sigma_k}\right)\frac{\partial k}{\partial x_j}\right] + \mu_t \frac{\partial u_i}{\partial x_j}\left(\frac{\partial u_i}{\partial x_j} + \frac{\partial u_j}{\partial x_i}\right) - \rho\varepsilon \tag{4}$$

Where k is turbulent kinetic energy

Dissipation equation of turbulent kinetic energy:

$$\frac{\partial}{\partial t}(\rho\varepsilon) + \frac{\partial}{\partial x_k}(\rho\varepsilon u_k) = \frac{\partial}{\partial x_k}\left[\left(\mu + \frac{\mu_t}{\sigma_\varepsilon}\right)\frac{\partial\varepsilon}{\partial x_k}\right] + \frac{c_1\varepsilon}{k}\mu_t\frac{\partial u_i}{\partial x_j}\left(\frac{\partial u_i}{\partial x_j} + \frac{\partial u_j}{\partial x_i}\right) - c_2\rho\frac{\varepsilon^2}{k} \tag{5}$$

2.3 Boundary conditions and algorithms

The boundary conditions were set as follows: the inlet was velocity inlet, the inlet velocity was variable and the temperature was set to be 303.15 K, the outlet was pressure outlet, the wall of tubes was set as no-slip wall, and the wall temperature was set as 290.65 K. The wall function was set as scalable wall function. The natural convection phenomenon caused by density change was ignored and the influence of fluid gravity was not considered. The working medium was PG-W mixture. Because the temperature change of the fluid was small, its material properties were assumed to be constant. SIMPLE scheme was adopted for the coupling of pressure-velocity. Second-order upwind scheme was applied for momentum, turbulent kinetic energy and turbulent dissipation rate. The convergent residual index was set as 1.0×10^{-3} except for energy and 1×10^{-6} for energy.

The thermophysical properties of PG-W mixture with different concentrations are different. Thermophysical properties of PG-W mixture with different concentrations are shown in table 2

Table 2 Thermophysical properties of PG-W mixture

Volume concentration	10%	20%	30%
Density (kg/m^3)	1005	1015	1024
Specific heat at constant pressure (J/kg/K)	4019	3994	3875
Thermal conductivity (W/m/K)	0.557	0.503	0.454
Dynamic viscosity (mPa·s)	1.11	1.52	2.18

2.4 Grid independence evaluation

Tetrahedral grids were used. Generated grid is shown in Fig. 2. ANSYS was used for analysis and meshing of the geometry. Heat transfer coefficient was calculated by using five kinds of grids, and the results are shown in Fig. 3. The boundary conditions and calculation settings are the same for each kind of grid.
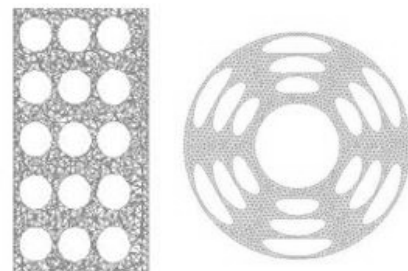

Fig. 2 Generated grid
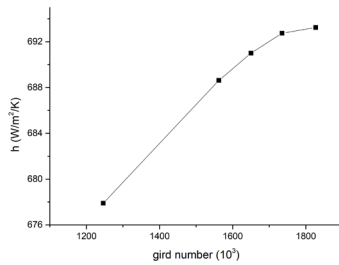
Fig. 3 Heat transfer coefficient of different kind of gird

As can be seen from Fig. 3, when the number of grids exceeds 1.65 million, the number of grids increases by 10%, and h increases by only 0.3%, which meets the engineering requirements. Considering the complexity of the model, the grid number selected was 1.775 million.

3. EXPERIMENT

3.1 Experimental set-up

Fig. 4 shows the experimental system. The PG-W mixture in tank was heated to 303.15 K and entered SWHE. After heat exchanging, it flew back to the tank. The volume flow rate was 0.4 m³/h, 0.5 m³/h, 0.6 m³/h, 0.7 m³/h or 0.8 m³/h. Water with a temperature range of 287.65 K to 288.65 K in water tank entered SWHE to transfer heat and then went away. The volume flow rate was 0.6 m³/h. The thermometer with a measuring range of 223.15 K to 473.15 K was used to measure temperature, the accuracy level of it was A, the measuring range of the flowmeter was 0.1 to 1 m³/h, the error was 1.5%.
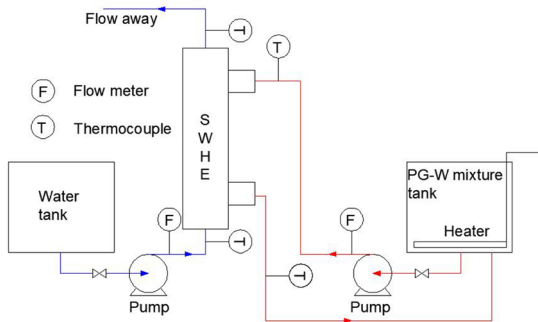
Fig. 4 Experimental system

3.2 Data reduction

The heat exchange of PG-W mixture is calculated as:
$$Q_c = c_p \rho q (T_{hin} - T_{hout}) \tag{6}$$

The average logarithmic temperature difference is calculated as:
$$\Delta T_m = \frac{\Delta T_{max} - \Delta T_{min}}{ln\left(\frac{\Delta T_{max}}{\Delta T_{min}}\right)} \tag{7}$$

$$\Delta T_{max} = T_{hin} - T_{cout}$$
$$\Delta T_{min} = T_{hout} - T_{cin}$$

The total heat transfer coefficient is calculated as:
$$h_a = \frac{Q_c}{A \Delta T_m} \tag{8}$$

The heat transfer coefficient in the tube side is calculated as follows.

The Re in the tube side is calculated as:
$$Re = d_i u \rho / \mu \tag{9}$$

The Re_c in the tube side is calculated as:
$$Re_c = 2300\left[1 + 8.6\left(\frac{d_i}{D_s}\right)^{0.45}\right] \tag{10}$$

if 100<Re<Re$_c$

$$Nu_t = 3.65 + 0.08\left[1 + 0.8\left(\frac{d_i}{D_s}\right)^{0.9}\right]Re^m Pr^{1/3} \tag{11}$$

$$m = 0.5 + 0.2903\left(\frac{d_i}{D_s}\right)^{0.194} \tag{12}$$

if Re$_c$ <Re<22000

$$Nu_t = 0.023\left[1 + 14.8(1 + \frac{d_i}{D_s})\left(\frac{d_i}{D_s}\right)^{1/3}\right]Re^m Pr^{1/3} \tag{13}$$

$$m = 0.8 - 0.22\left(\frac{d_i}{D_s}\right)^{0.1} \tag{14}$$

if 22000 <Re

$$Nu_t = 0.023\left[1 + 3.6(1 - \frac{d_i}{D_s})\left(\frac{d_i}{D_s}\right)^{0.8}\right]Re^{0.8} Pr^{1/3} \tag{15}$$

The heat transfer coefficient in the tube side is calculated as:
$$h_t = Nu_t \lambda_w / d_i \tag{16}$$

The heat transfer coefficient in the shell side is calculated as:
$$\frac{1}{h_s} = d_o/d_i\left[\frac{1}{h_a} - \frac{1}{h_t} - \frac{d_o \, ln(d_o/d_i)}{2\pi\lambda_s}\right] \tag{17}$$

3.3 Uncertainty analysis

Since there was uncertainty in the measurement, the errors of these parameters must be passed to the heat transfer coefficient, the maximum error of h is calculated as:

$$E(\delta h) = \sqrt{\left(\frac{\delta Q}{Q}\right)^2 + 4\left(\frac{\delta(\Delta T_m)}{\Delta T_m}\right)^2} \tag{18}$$

The maximum errors are shown in Table 3.

**Table 3** Maximum error

10% concentration			
Volume flow rate (m³/h)	Error of temperature measuring instrument (K)	Error of flow rate measuring instrument (m³/h)	Maximum error of h (%)
0.4	0.1	0.015	2.4
0.5	0.1	0.015	2.6
0.6	0.1	0.015	2.7
0.7	0.1	0.015	2.8
0.8	0.1	0.015	3.1
20% concentration			
Volume flow rate (m³/h)	Error of temperature measuring instrument (K)	Error of flow rate measuring instrument (m³/h)	Maximum error of h (%)
0.4	0.1	0.015	2.5
0.5	0.1	0.015	2.6
0.6	0.1	0.015	2.9
0.7	0.1	0.015	3
0.8	0.1	0.015	3.2
30% concentration			
Volume flow rate (m³/h)	Error of temperature measuring instrument (K)	Error of flow rate measuring instrument (m³/h)	Maximum error of h (%)
0.4	0.1	0.015	2.5
0.5	0.1	0.015	2.6
0.6	0.1	0.015	2.9
0.7	0.1	0.015	3.1
0.8	0.1	0.015	3.3

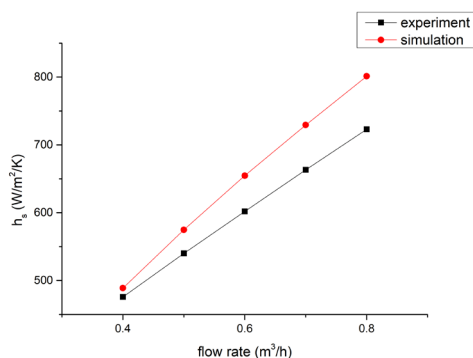As shown in table 3, the maximum error of h is within 5%.

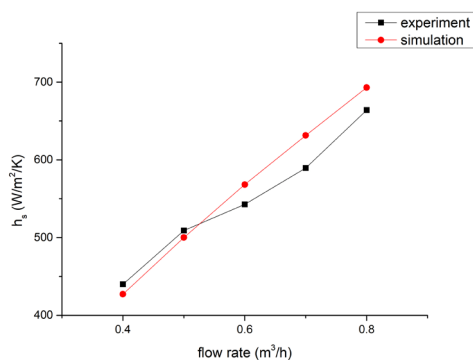### 3.4 Experimental verification

The comparison between the experimental results and the simulation results is shown in Fig. 5.

3
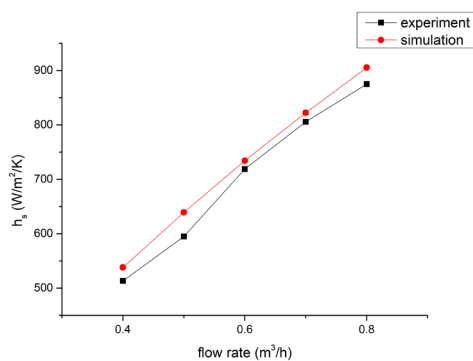
(a) 10% concentration
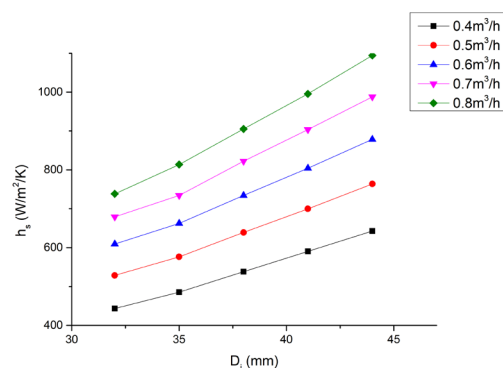

(b) 20% concentration

(c) 30% concentration

Fig. 5 Experimental results compared with simulation results

As shown in Fig. 5, the simulation results are close to the experimental results, with an average difference of 5.3%, the largest difference is 10.8%.
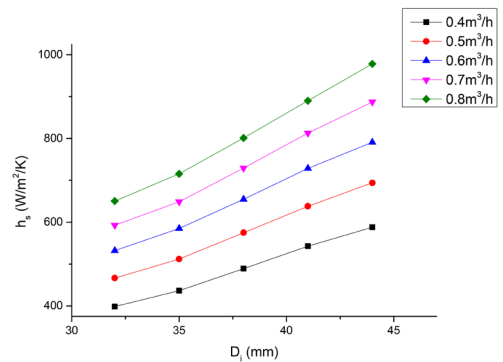
4. RESULTS AND DISCUSSION

Fig. 6 shows the change of h_s with the center core diameter under different volume flow rates and concentrations.
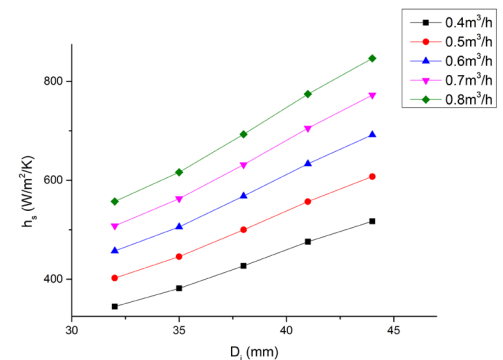
As can be seen from Fig. 6, h_s increases with the increase of D_i at three concentrations. When the concentration is 10%, the D_i increases from 32mm to 44mm, and h_s increases by 45% on average. When the concentration is 30%, the D_i increases from 32mm to 44mm, and h_s increases by 51% on average. Therefore, the higher the concentration is, the greater the influence of the D_i on h_s is. This is because as the D_i increasing, the areas of fluid contacting with tubes will increase, and the overall heat transfer efficiency will be higher, as shown in Fig.7. When D_i is small, some fluid flows between the tubes and wall of center core.

(a) 10% concentration

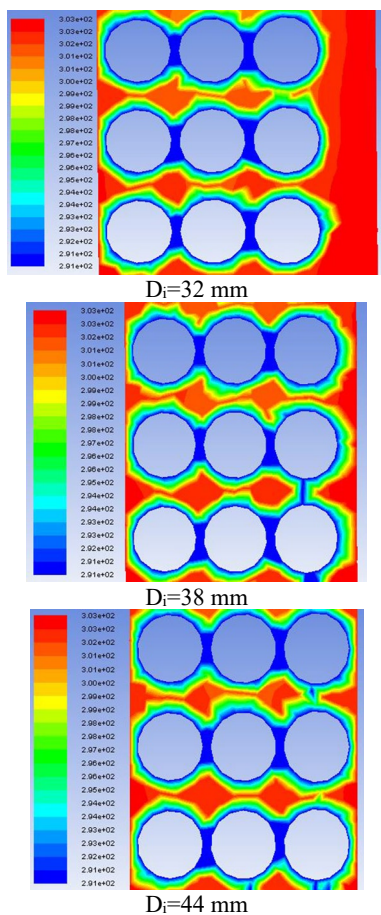(b) 20% concentration

(c) 30% concentration

Fig. 6 Heat transfer coefficient versus with center core diameter under different volume flow rate and concentration, respectively

Fig. 8 shows the change of h_s with the longitudinal spacing of tubes under different volume flow rates and concentrations.
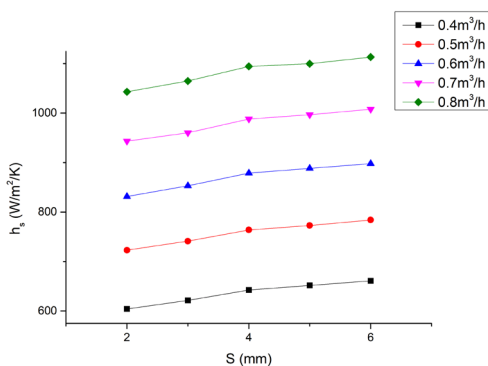
As can be seen from Fig. 8, h_s increases with the increase of S at three concentrations. When the concentration is 10%, S increases from 2 mm to 6 mm, h_s increases by 7.9% on average; when the concentration is 30%, S increases from 2 mm to 6 mm, h_s increases by 2.3% on average. Therefore, the higher the concentration is, the less the influence of the S on h_s is. This is because the greater the S is, the faster the fluid velocity between the tubes is, as shown in Fig. 9. The fluid flushing wall reduces the boundary layer thickness and improves the heat transfer efficiency.

Table 4 Heat exchange and heat transfer area under different d_o (concentration is 10%, volume flow rate is 0.6 m³/h)
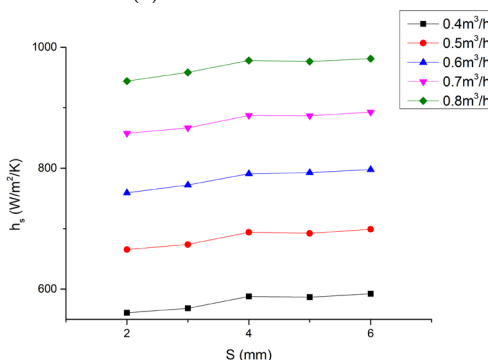
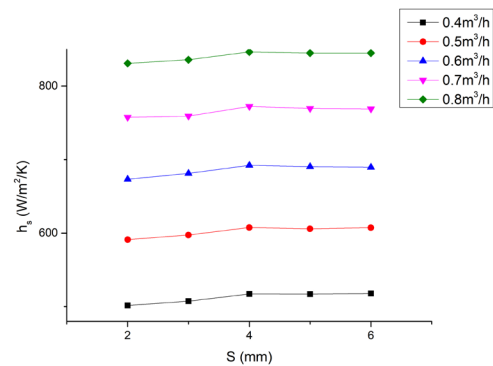| d_o（mm）	6	7	8	9	10
Heat exchange（W）	5370	5298	5189	5060	4939
Heat transfer area (m²)	0.633	0.655	0.667	0.674	0.678

D_i=32 mm

D_i=38 mm

D_i=44 mm

Fig. 7 Temperature nephogram under different D_i (concentration is 30%, volume flow rate is 0.6 m³/h)
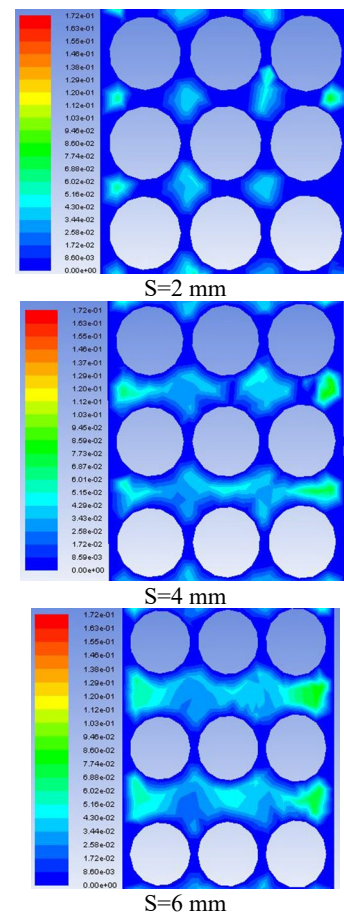

(a) 10% concentration
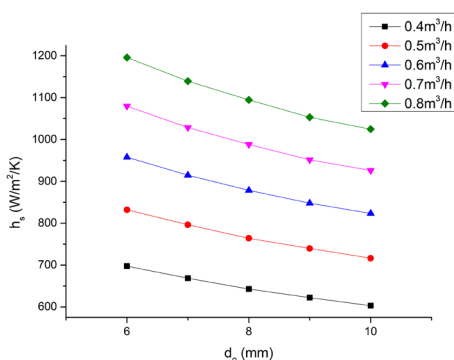

(b) 20% concentration

(c) 30% concentration

Fig. 8 Heat transfer coefficient versus with longitudinal spacing of tubes under different volume flow rate and concentration, respectively


S=2 mm

S=4 mm

S=6 mm

Fig. 9 Flow nephogram under different S (concentration is 10%, volume flow rate is 0.6 m³/h)

Fig. 10 shows the change of h_s with the tube outer diameter under different volume flow rates and concentrations. As can be seen from Fig. 10, h_s decreases with the increase of d_o at three concentrations. When the concentration is 10%, d_o increases from 6 mm to 10 mm, and h_s decreases by 14% on average. When the concentration is 30%, d_o increases from 6 mm to 10 mm, and h_s decreases by 15% on average. Therefore, the higher the concentration is, the greater the influence of d_o on h_s is. This is because the heat transfer area increases with the increase of d_o, but the heat exchange decreases, as shown in table 4, so the heat transfer coefficient decreases.

(a) 10% concentration
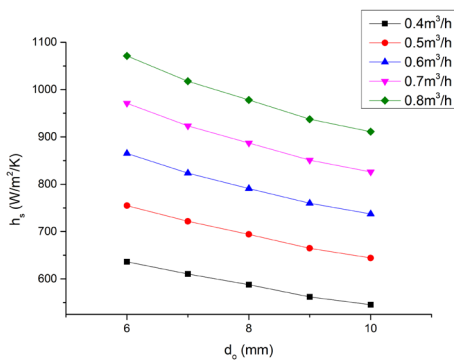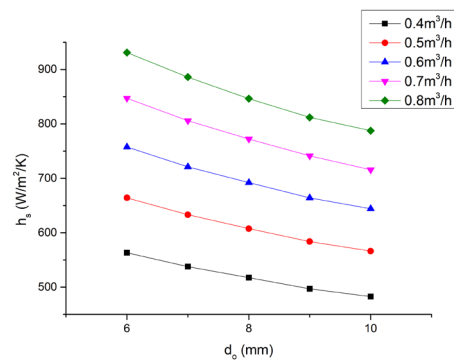
(b) 20% concentration

(c) 30% concentration

Fig. 10 Heat transfer coefficient versus with tube outer diameter under different volume flow rate and concentration, respectively
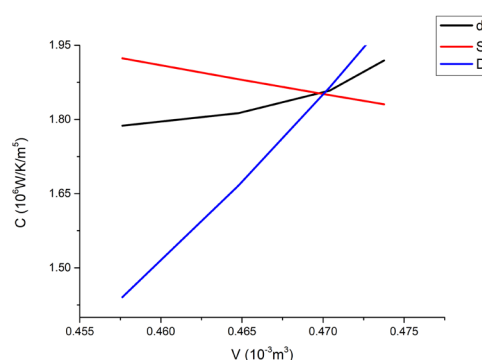

(a)　10% concentration

(b)　20% concentration

(c)　30% concentration

Fig. 11 C changes with V

5.   ECONOMIC ANALYSIS

The cost of SWHE includes material cost and processing cost. Only material cost is considered here. Assume that the shell, center core, and tubes are of the same material. Changing the structure of the SWHE will lead to a change in the amount of material, thus changing the cost. Since the density of the same material is the same, the volume of the material of the same amount is the same.
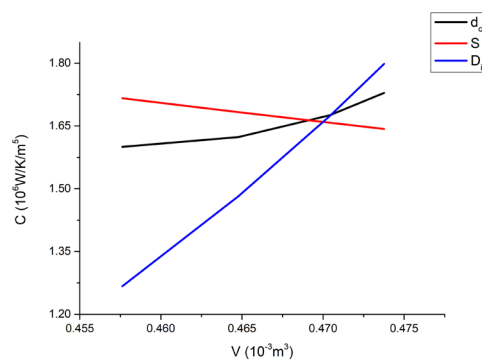
The economic index is defined as follows:

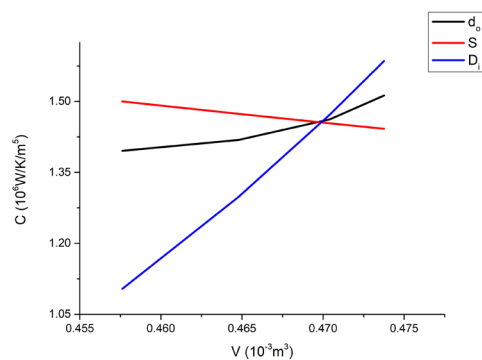$$C = \left(\sum_{0.4}^{0.8} \frac{h_i}{V_i} \right) / 5 \qquad (19)$$

where, h_i represents the heat transfer coefficient, V_i represents the material volume, and subscript i represents the volume flow rate. Since it is hard to determine the running time taken by each volume flow rate in practice, it is assumed that the weight of each volume flow rate is equal. The change of C with V at different concentrations of PG-W mixture is shown in Fig. 11.

As shown in Fig. 11, with the increase of material consumption, the heat transfer coefficient can be increased if the material is used to change the tube outer diameter and center core diameter, while the heat transfer coefficient can be decreased if the material is used to change longitudinal spacing of tubes. Since the line representing the center core diameter in Fig.11 has a higher slope, changing center core diameter has a higher cost performance compared to changing the tube outer diameter. The above conclusions are not affected by the change of concentration of PG-W mixture.

6.   CONCLUSIONS

The heat transfer characteristic of PG-W mixture in the shell side of SWHE was studied by numerical simulation. The average difference between the simulated results and the experimental results was 5.3%. The heat transfer characteristics of PG-W mixture with different concentration in the shell side of SWEH with different center core diameter, different longitudinal spacing of tube and different tube outer diameter were investigated. Finally, the economic index was established to evaluate the economy of SWHE. The main conclusions are as follows:

- The large center core diameter leads to a high heat transfer coefficient due to more fluid contact with the tubes. In addition, the greater the concentration of PG-W mixture is, the greater the influence of the center core diameter on the heat transfer coefficient will be.
- The increase of the longitudinal spacing of tubes has positive effect on heat transfer characteristics of PG-W mixture because the larger longitudinal spacing of tubes increases the fluid velocity between the tubes and reduces the boundary layer thickness. The influence of longitudinal spacing of tubes on heat transfer coefficient increases when concentration decreases.
- Smaller tube outer diameter leads to more heat exchange, so the heat transfer coefficient is larger. The influence of tube outer diameter on heat transfer coefficient increases with the increase of concentration.
- Adding materials for changing center core diameter and tube outer diameter will improve economic index. While adding materials for changing longitudinal spacing of tubes will reduce economic index. Comparing with changing tube outer diameter, changing center core diameter has higher cost performance.

NOMENCLATURE

A	heat transfer area (m^2)
c_p	specific heat capacity of PG-W mixture (J/kg/K)
d_i	tube inner diameter (m)
d_o	tube outer diameter (m)
D_s	coil diameter (m)
D_i	center core diameter (m)
D_o	outer diameter of SWHE (m)
h_a	total heat transfer coefficient (W/m^2/K)
h_s	heat transfer coefficient in the shell side (W/m^2/K)
h_t	heat transfer coefficient in the tube side (W/m^2/K)
H	length of SWHE (m)
l	horizontal spacing of tubes (m)
Nu	Nusselt number (dimensionless)
Pr	Prandtl number (dimensionless)
q	flow (m^3/h)
Qc	heat exchange (W)
Re	Reynolds number (dimensionless)
S	longitudinal spacing of tubes (m)
T_m	average logarithmic temperature (K)
T_{cin}	inlet temperature of cold fluid (K)
T_{cout}	outlet temperature of cold fluid (K)
T_{hin}	inlet temperature of hot fluid (K)
T_{hout}	outlet temperature of hot fluid (K)
u	velocities (m/s)
x,y	coordinates (m)
Greek Symbols	
ρ	density (kg/m^3)
λ_s	thermal conductivity of steel (W/m/K)
λ_w	thermal conductivity of water (W/m/K)
μ	viscosity (N·s/m^2)
Subscripts	
s	shell side
t	tube side

REFERENCES

Ahmadi R., Hosseini M. J., Ranjbar A. A., Bahrampoury R., 2018, "Phase change in spiral coil heat storage systems," *Sustainable Cities and Society,* **38**, 145-157.
https://doi.org/10.1016/j.scs.2017.12.026

Amnart B., Withada J., 2018, "Numerical predictions on flow and heat transfer in heat exchanger tube equipped with various flow attack angles of inclined-wavy surface," *Frontier in Heat and Mass Transfer,* **11**, 10.
http://dx.doi.org/10.5098/hmt.11.10

Daghigh R., Zandi P., 2018, "Experimental analysis of heat transfer in spiral coils using nanofluids and coil geometry change in a solar system," *Applied Thermal Engineering,* **145**, 295-304.
https://doi.org/10.1016/j.applthermaleng.2018.09.053

Duan Z., Ren T., Ding G. L., Chen. J., Pu. H., 2016, "A dynamic model for FLNG spiral wound heat exchanger with multiple phase-change streams based on moving boundary method," *Journal of Natural Gas Science and Engineering,* **34**, 657-669.
https://doi.org/10.1016/j.jngse.2016.07.036

Ghorbani N., Taherian H., Gorji M., Mirgolbabaei H., 2010, "Experimental study of mixed convection heat transfer in vertical helically coiled tube heat exchangers," *Experimental Thermal and Fluid Science,* **34**(7), 900-905.
https://doi.org/10.1016/j.expthermflusci.2010.02.004

Gupta A., Kumar R., Gupta A., 2014, "Condensation of R-134a inside a helically coiled tube-in-shell heat exchanger," *Experimental Thermal and Fluid Science,* **54**, 279-289.
https://doi.org/10.1016/j.expthermflusci.2014.01.003

Han H. Z., Li B. X., Shao. W., 2016, "Effect of flow direction for flow and heat transfer characteristics in outward convex asymmetrical corrugated tubes," *International Journal of Heat and Mass Transfer,* **92**, 1236-1251.
https://doi.org/10.1016/j.ijheatmasstransfer.2014.11.076

Jian G. P., Wang S. M., Sun L. J., Wen J., 2019, "Numerical investigation on the application of elliptical tubes in a spiral-wound heat exchanger used in LNG plant," International Journal of Heat and Mass Transfer, 130, 333-341.
https://doi.org/10.1016/j.ijheatmasstransfer.2018.10.089

Jian G. P., Wang S. M., Sun L. J., Wen J., Tu J. Y., 2020, "Experimental study of the effects of key geometry parameters on shell-side vapor condensation of spiral-wound heat exchangers," *Applied Thermal Engineering,* **166**, 114731.
https://doi.org/10.1016/j.applthermaleng.2019.114731

Klotzbücher T., Kappler A., Straub K. L., Haderlein S. B., 2007, "Biodegradability and groundwater pollutant potential of organic anti-freeze liquids used in borehole heat exchangers," *Geothermics,* **36**(4), 348-361.
https://doi.org/10.1016/j.geothermics.2007.03.005

Mestemaker B. T. W., Castro M. B. G., H.N. van den Heuvel, K. Visser, 2020, "Dynamic simulation of a vessel drive system with dual fuel engines and energy storage," *Energy,* **194**, 116792.
https://doi.org/10.1016/j.energy.2019.116792

Mirgolbabaei H., 2018, "Numerical investigation of vertical helically coiled tube heat exchangers thermal performance," *Applied Thermal Engineering,* **136**, 252-259.
https://doi.org/10.1016/j.applthermaleng.2018.02.061

Mostafazade A. A., Afshin H., 2019, "Development of Nusselt number and friction factor correlations for the shell side of spiral-wound heat exchangers," *International Journal of Thermal Sciences,* **139**, 105-117.
https://doi.org/10.1016/j.ijthermalsci.2019.01.038

Neeraas B. O., Fredheim A. O., Aunan B., 2004, "Experimental data and model for heat transfer, in liquid falling film flow on shell-side, for spiral-wound LNG heat exchanger," *International Journal of Heat and Mass Transfer,* **47**, 3565-3572.
https://doi.org/10.1016/j.ijheatmasstransfer.2004.01.009

Park H., Lee S., Jeong J., Chang D., 2018, "Design of the compressor-assisted LNG fuel gas supply system," *Energy,* **158**, 1017-1027.
https://doi.org/10.1016/j.energy.2018.06.055

Pawar S. S., Sunnapwar V. K., 2014, "Experimental and CFD investigation of convective heat transfer in helically coiled tube heat exchanger," *Chemical Engineering Research and Design,* **92**, 2294-2312.
https://doi.org/10.1016/j.cherd.2014.01.016

Rafiq M., Patrick H. O., 2019, "Numerical and experimental investigations of natural convective heat transfer from two-sided diagonally inclined square plates having a finite thickness," *Frontier in Heat and Mass Transfer,* **13**, 7.
http://dx.doi.org/10.5098/hmt.13.7

Ren Y., Cai W. H., Chen J., Lu L. Y., Wang J. S., Jiang Y. Q., 2018, "The heat transfer characteristic of shell-side film flow in spiral wound heat exchanger under rolling working conditions," *Applied Thermal Engineering,* **132**, 233-244.
https://doi.org/10.1016/j.applthermaleng.2017.12.092

Saydam V., Parsazadeh M., Radeef M., Duan X. L., 2019, "Design and experimental analysis of a helical coil phase change heat exchanger for thermal energy storage," *Journal of Energy Storage,* **21**, 9-17.
https://doi.org/10.1016/j.est.2018.11.006

Solanki A. K., Kumar R., 2019, "Two-phase flow condensation heat transfer characteristic of R-600a inside the horizontal smooth and dimpled helical coiled tube in shell type heat exchanger," *International Journal of Refrigeration,* **107**, 155-164.
https://doi.org/10.1016/j.ijrefrig.2019.07.017

Wang G. H., Wang D. B., Peng X., Han L. L., Xiang S., Ma F., 2019, "Experimental and numerical study on heat transfer and flow characteristics in the shell side of helically coiled trilobal tube heat exchanger," *Applied Thermal Engineering,* **149**, 772-787.
https://doi.org/10.1016/j.applthermaleng.2018.11.055

Wang S. M., Jian G. P., Wang J. R., Sun L. J., Wen J., 2018, "Application of entransy-dissipation-based thermal resistance for performance optimization of spiral-wound heat exchanger," *International Journal of Heat and Mass Transfer,* **116**, 743-750.
https://doi.org/10.1016/j.ijheatmasstransfer.2017.09.061

Wang Z. Y., Zhou Z. X., Yang M., 2020, "Double diffusive natural convection in open cavity under the soret and dufour effects," *Frontier in Heat and Mass Transfer,* **14**, 13.
https://doi.org/10.5098/hmt.14.13

Weikl M. C., Braun K., Weiss J., 2014, "Coil-wound Heat Exchangers for Molten Salt Applications," *Energy Procedia,* **49**, 1054-1060.
https://doi.org/10.1016/j.egypro.2014.03.113

Yu J. W., Jiang Y. Q., Cai W. H., Li F. Z., 2018, "Forced convective condensation flow and heat transfer characteristics of hydrocarbon mixtures refrigerant in helically coiled tubes," *International Journal of Heat and Mass Transfer,* **124**, 646-654.
https://doi.org/10.1016/j.ijheatmasstransfer.2018.03.097

Zhu J. L., Sun C. Z., Li Y. X., Shan W. G., 2019, "Experiment on adaptability of feed gas flow rate and sea conditions on FLNG spiral wound heat exchanger," *International Journal of Heat and Mass Transfer,* **138**, 659-666.
https://doi.org/10.1016/j.ijheatmasstransfer.2019.04.087